A layered erythromyeloid ontogeny ensures timely supply of erythrocytes and macrophages during development

Ramy Elsaid, Aya Mikdache, Patricia Diabangouaya, Gwendoline Gros, Pedro P Hernández

A layered erythromyeloid ontogeny ensures timely supply of erythrocytes and macrophages during development

Ramy Elsaid[1,*], Aya Mikdache[1], Patricia Diabangouaya[1,#], Gwendoline Gros[1,#] and Pedro P. Hernández[1,*].

[1]Institut Curie, PSL Research University CNRS UMR 3215, INSERM U934, 26 Rue d'Ulm, 75248 Paris Cedex 05, France.

# These authors contributed equally to this work.

*Corresponding author. Email: pedro.hernandez-cerda@curie.fr (P.P.H.) and ramy.elsaid@curie.fr (R.E.).

Short running title: Layered erythromyeloid ontogeny in zebrafish

Highlights

Primitive hematopoietic progenitors give rise and sustain embryonic erythromyeloid lineages.

Definitive hematopoietic progenitors show a late contribution to macrophages and erythrocytes during development.

Embryos show a layered ontogeny of macrophages that ensures their abundance for a timely contribution to tissue homeostasis and repair.

Selective ablation of definitive macrophages does not impair tail fin regeneration during early larval developmental stages.

Abstract

In all organisms studied, from flies to humans, blood cells emerge in several sequential waves and from distinct hematopoietic origins. However, the relative contribution of these ontogenetically distinct hematopoietic waves to embryonic blood lineages and to tissue regeneration during development is yet elusive. Here, using a lineage-specific 'switch and trace' strategy in the zebrafish embryo, we report that the definitive hematopoietic progeny barely contributes to erythrocytes and macrophages during early development. Lineage tracing further show that ontogenetically distinct macrophages exhibit differential recruitment to the site of injury based on the developmental stage of the organism. We further demonstrate that primitive macrophages can solely maintain tissue regeneration during early larval developmental stages after selective ablation of definitive macrophages. Our findings highlight that the sequential emergence of hematopoietic waves in embryos ensures the abundance of blood cells required for tissue homeostasis and integrity during development

Keywords

Ontogeny; Hematopoiesis; Lineage tracing; Regeneration; Zebrafish

Introduction

Hematopoiesis is a complex biological process by which all mature blood lineages are generated. In mammals, hematopoiesis originates from distinct blood progenitors that arise during development resulting in a layered organization of the immune system (Elsaid et al., 2020). In mice, the first wave, also called primitive wave, starts in the extra-embryonic microenvironment of the yolk sac (YS) around embryonic day (E) 7 (Palis et al., 1999; Kingsley et al., 2004; Palis et al., 2001; Soares-da-Silva et al., 2021). Around E8.25, the YS also harbors endothelial-derived multipotent erythro-myeloid progenitors (EMPs) which represent the first definitive wave of hematopoiesis (Hoeffel et al., 2015; Gomez Perdiguero et al., 2015; Bertrand et al., 2005; Gentek et al., 2018; Frame et al., 2016). At E9.5, other intra-embryonic definitive hematopoietic progenitors emerge in the major arteries and they are the main source of adult hematopoietic stem cells (HSCs) in the bone marrow (BM) (Cumano et al., 1996; Medvinsky and Dzierzak, 1996; Busch et al., 2015). These progenitors emerge through an endothelial-to-hematopoietic transition mechanism (EHT) (Bertrand et al., 2010; Boisset et al., 2010; Kissa and Herbomel, 2010b). At E10.5, the fetal liver (FL), the main hematopoietic organ during embryonic development, harbors progenitors of dual origin derived from both definitive and primitive hematopoietic progenitors (McGrath et al., 2015a). As in mammals, zebrafish hematopoiesis also consists of multiple waves that emerge at distinct anatomical locations (Elsaid et al., 2020). In the zebrafish embryo, primitive hematopoiesis emerges intra-embryonically around 11 hours post-fertilization (hpf) in the rostral blood island (RBI) and the posterior lateral mesoderm (PLM) and generates primitive erythrocytes and myeloid cells (Elsaid et al., 2020; Herbomel et al., 2001). Recently, the RBI was shown to be major source of embryonic microglia (Ferrero et al., 2018; Xu et al., 2015). Other definitive or endothelial-derived hematopoietic waves are also produced in the developing organism (Elsaid et al.,

2020). One of them is a transient wave that emerges from the posterior blood island (PBI) at 24-30 hpf via EHT and gives rise to EMPs like those in mammals (Bertrand et al., 2007; Ferrero et al., 2018; Tian et al., 2017). At 36 hpf, other waves of HSCs and HSC-independent progenitors emerge from the dorsal aorta (DA) via EHT (Bertrand et al., 2010; Kissa and Herbomel, 2010b). These DA-derived hematopoietic progenitors then migrate to the caudal hematopoietic tissue (CHT) (Murayama et al., 2006). By 4 days post-fertilization (dpf), hematopoietic stem and progenitor cells migrate to the kidney marrow, the BM counterpart in zebrafish, where they reside and differentiate to all blood cell lineages, establishing the adult hematopoietic system (Murayama et al., 2006). Therefore, due to its similarity to mammalian hematopoiesis, the zebrafish is an excellent model to study the ontogeny of different hematopoietic waves during development.

Although it is well characterized that blood cells are produced in sequential and overlapping waves (Elsaid et al., 2020), little is known about their contribution to different hematopoietic lineages during development. However, recent studies in mice and in zebrafish suggest that immune and blood cells might have distinct origins throughout life (Hoeffel et al., 2015; Ferrero et al., 2018; Xu et al., 2015; Gentek et al., 2018; Gomez Perdiguero et al., 2015; Soares-da-Silva et al., 2021). Independent reports support the notion that definitive hematopoiesis sustains embryonic blood lineages (Tian et al., 2017; Ulloa et al., 2021; Patel et al., 2022; Stachura and Traver, 2011). However, primitive hematopoietic progenitors give rise also to the erythromyeloid lineage and it is yet unknown to what extent these progenitors contribute to embryonic blood lineages. This is mainly due to the lack of specific markers for primitive hematopoietic progenitors in mammals (Elsaid et al., 2020; Ferrero et al., 2018; Xu et al., 2015; McGrath et al., 2015b).

The difficulty in accurately tracing the output of each wave in mammalian animal models has hindered the full understanding of immune cell ontogeny. Recent studies in zebrafish showed that embryonic and larval microglia originate from the RBI while adult microglia and other adult macrophages arise from the ventral wall of dorsal aorta (VDA) (Xu et al., 2015; He et al., 2018; Ferrero et al., 2018). Despite their elegant experimental designs, only microglia and adult macrophages origins were tested, without exploring the contribution of primitive hematopoiesis to the embryonic/larval erythromyeloid lineage during tissue homeostasis and regeneration.

In this study, we used the unique strengths of the zebrafish embryo to perform temporarily resolved lineage tracing combined with live imaging to investigate the embryonic erythromyeloid lineage ontogeny *in vivo*. We unveiled that embryonic erythrocyte and macrophage lineages originate from primitive hematopoietic progenitors. In contrast, definitive hematopoietic waves contribution to the erythromyeloid lineage occurred only at the larval developmental stage. We further showed that upon tissue injury only primitive, but not definitive, macrophages are recruited to the site of injury during embryonic development. While both ontogenetically distinct macrophage populations were recruited to the site of injury at early larval developmental stages, primitive macrophages were recruited to the damage site earlier than their definitive counterparts. Our results also suggest that primitive macrophages maintain tissue regeneration during early larval developmental stages after selective ablation of definitive macrophages. Combined, our study reveals that the sequential emergence of hematopoietic waves ensures the abundance of macrophages and erythrocytes required for tissue homeostasis and integrity during development.

Results and discussion

Erythrocytes originate from primitive hematopoietic progenitors during embryonic development.

To set up a strategy to distinguish between primitive and definitive hematopoietic progenitors based on their tissue of origin, we used an endothelial-specific tamoxifen-inducible transgenic line *Tg(fli1a:CreERT2)* (Sánchez-Iranzo et al., 2018) in combination with different hematopoietic lineage-specific switch and trace lines (Carney and Mosimann, 2018). All definitive hematopoietic progenitors, including HSCs and EMPs, are generated as early as 24 hpf from endothelial progenitors (Bertrand et al., 2010; Kissa and Herbomel, 2010a; Tian et al., 2017; Henninger et al., 2017; Ulloa et al., 2021; Bertrand et al., 2007). Thus, our inducible labeling strategy at 24 hpf will label exclusively definitive hematopoietic progenitors as they emerge without labeling primitive hematopoietic progenitors. To assess the efficiency of our labeling strategy, we combined the *Tg(fli1a:CreERT2)* line with two different independent transgenic lines, the lymphocyte-specific *Tg(lck:loxP-DsRedx-loxP-GFP)* (Tian et al., 2017; Langenau et al., 2004) line (supplemental Figure 1A) and the *Tg(coro1a:loxP-DsRedx-loxP-GFP)* line which labels all leukocytes(Xu et al., 2015; Li et al., 2012) (supplemental Figure 1D). We found that 80% of thymocytes in the thymus, which have only a definitive hematopoietic origin (Tian et al., 2017; Elsaid et al., 2021), were labelled using either the *Tg(lck:loxP-DsRedx-loxP-GFP)* (supplemental Figure 1B-C) or the *Tg(coro1a:loxP-DsRedx-loxP-GFP)* lines (supplemental Figure 1E-F), indicating the high labelling efficiency of our system.

To determine the origin of erythrocytes during embryonic development and early larval stages, we combined the *Tg(fli1a:CreERT2)* line with the erythrocyte-specific *Tg(α/β$_{a2}$-globin:loxP-DsRedx-loxP-GFP)* line (referred to hereafter as globin:switch) (Tian et al., 2017;

Ganis et al., 2012). In double transgenic zebrafish, 4-OH-tamoxifen (4-OHT) induces cre recombination and removes the DsRed cassette, leading to permanent GFP expression in *fli1a*$^{+}$-derived erythroid progeny (Figure 1A). To determine the contribution of definitive hematopoietic progenitors to erythropoiesis during early stages of development, we exposed embryos to either 4-OHT or ethanol (EtOH) starting at 24 hpf to label the aortic-endothelium-derived definitive hematopoietic progenitors (Bertrand et al., 2010; Kissa and Herbomel, 2010a; Tian et al., 2017), and then monitored GFP^{+} definitive erythrocytes via live imaging (Figure 1B and supplemental video 1). Primitive hematopoietic progenitors robustly generated erythrocytes from early embryonic stages (Figure 1B). In contrast, GFP^{+} definitive erythrocytes started to emerge after 2 dpf, accumulated in the CHT region starting at 4 dpf (Figure 1C) and their contribution to the erythrocyte pool was not appreciable until later larval developmental stages (~21 dpf, Figure 1C-F).

Using this labeling strategy, we demonstrated that under physiological conditions, definitive hematopoietic progenitors barely contribute to erythropoiesis during early stages of development. These results indicate that erythrocytes emerge in a layered organization during embryonic and early larval stages as in mammals (Soares-da-Silva et al., 2021), and that primitive hematopoietic progenitors generate a sufficient number of erythrocytes to sustain embryonic survival and tissue homeostasis (Palis, 2014).

Embryonic macrophages originate exclusively from primitive hematopoietic progenitors

To assess the contribution of definitive hematopoietic progenitors to the embryonic macrophage pool, we marked the latter by combining the *Tg(fli1a:CreERT2)* line with the macrophage-specific *Tg(mpeg1:LoxP-DsRedx-LoxP-GFP-NTR)* line (referred to hereafter as

196 mpeg1:switch) (Lin et al., 2019; Ellett et al., 2011). As aforementioned, 4-OHT-induced cre
197 recombination leads to permanent GFP expression in *fli1a*$^{+}$-derived macrophages progeny
198 (Figure 2A). Using this system, embryonic microglia cells, which are known to be of primitive
199 hematopoietic origin in zebrafish (Xu et al., 2015; Ferrero et al., 2018), were not labelled,
200 indicating the precision of this labelling system (supplemental figure 2A-B). While primitive
201 macrophages contributed robustly to the embryonic macrophage pool, we found that
202 definitive hematopoietic progenitors minimally contribute to macrophages during early
203 developmental stages, akin to erythrocytes ontogeny (Figure 2B). We showed further that
204 GFP^{+} definitive macrophages started to emerge after 2 dpf and gradually increased in
205 numbers in the CHT region (Figure 2B and E) with a delayed modest contribution to the
206 macrophage pool in the periphery starting after 4 dpf (Figure 2B-D). GFP^{+} definitive
207 macrophages contributed robustly to peripheral macrophages by 16 dpf, suggesting a distinct
208 differentiation kinetics of primitive and definitive macrophages throughout development
209 (Figure 2C).

210 Altogether, our lineage tracing experiments show that aortic endothelium derived
211 hematopoietic progenitors are barely contributing to embryonic erythroid and myeloid
212 lineages (Figures 1 and 2). These data demonstrate that erythromyeloid lineages are mainly
213 sustained by primitive hematopoietic progenitors during early developmental stages under
214 physiological conditions.

215

216 Ontogenically distinct macrophages are differentially recruited to the site of injury throughout
217 development.

218 It has been recently reported that distinct macrophage subpopulations play different roles to

promote tail regeneration after amputation (Wynn and Vannella, 2016; Morales and Allende, 2019). However, whether ontogenetically distinct macrophages display different functions and recruitment behaviors to the site of injury remains poorly understood. Our tracing experiments suggested that the definitive hematopoietic progenitors barely contribute to the macrophage pool during early developmental stages under homeostasis. Therefore, we sought to analyze if macrophages of distinct origins are recruited in a differential manner to the damage site at different developmental stages. To track ontogenetically distinct macrophages recruitment upon injury, we used the same strategy applied to trace them under homeostasis (Figure 3A). We analyzed macrophages recruitment to the damaged site in embryos (2 dpf) and larvae (5 dpf) since our lineage tracing experiments showed a different abundance of ontogenetically distinct macrophages at these developmental stages (Figure 2). We observed that only primitive macrophages were recruited to the site of injury in embryos upon tail amputation (Figure 3B-C and supplemental Figure 3A). We then analyzed macrophage recruitment to the damage site in larvae, where both primitive and definitive macrophage populations coexist in the periphery. We did not observe differences in the recruitment of both primitive and definitive macrophages to the damage site 24 hours post amputation (hpa) with a slight increase in the number of definitive macrophages 48 hpa (Figure 3D-E and supplemental Figure 3B). Altogether, these results suggest that primitive macrophages can alone maintain embryonic tissue homeostasis while both macrophage populations are recruited to the damaged site and contribute to tail fin regeneration in the larvae.

Previous reports showed that the first recruited macrophages play an important role in proper tail fin regeneration (Morales and Allende, 2019; Nguyen-Chi et al., 2017; Petrie et al., 2014), therefore, we further analyzed which macrophage population is recruited first to the

site of injury. We found that primitive macrophages are recruited earlier than their definitive counterparts (Figure 3F-G). Since our observation of a delay in the recruitment of definitive macrophages could be the result of differences in the number of primitive and definitive macrophages in the periphery at the time of injury, we attempted to normalize their numbers. Data was normalized by dividing the number of each recruited macrophage subpopulation by their total number in the tail of the same larvae (Morales and Allende, 2019). After normalization, we still observed that primitive macrophages are recruited earlier compared to their definitive counterparts (Figure 3G). These data indicate that primitive macrophages, as the first arrivals to the damage site, may have a specific role in the regeneration process after amputation during development. Collectively, these results suggest that a layered ontogeny of macrophages ensures their abundance for a timely contribution to tissue homeostasis and regeneration.

Primitive macrophages solely maintain tissue regeneration during early larval developmental stages after selective ablation of definitive macrophages.

To evaluate the contribution of ontogenetically distinct macrophages to the regeneration of the damaged tissue, we used the aforementioned strategy to trace and deplete macrophages in a wave-specific manner during the regeneration process (Figure 4A). We used the mpeg1 switch line *Tg(mpeg1:loxP-dsRed-loxP-eGFP-NTR)* that allows selective ablation of macrophages based on their origin. In this line, the expression of bacterial nitroreductase (NTR) is under the control of the *mpeg1* promoter (Ellett et al., 2011). Thus, the NTR will be expressed exclusively in the traced macrophages, thereby, traced macrophages could be ablated by metronidazole (MTZ) treatment (Curado et al., 2008). Following this approach, we evaluated the contribution of definitive macrophages selectively upon tissue injury. To assess

the efficiency of the NTR-MTZ system, we quantified the number of primitive and definitive macrophages in the tail after treatment with either DMSO or MTZ for 48 hours from 4 to 6 dpf. We found that while primitive macrophages were not affected by the MTZ treatment, definitive macrophages were significantly reduced after 48 hours of MTZ treatment (Figure 4B-C).

We next performed tail fin amputation in 5 dpf larvae that was treated with either DMSO or MTZ from 4-6 dpf to ensure ablation of definitive macrophages through the regeneration process. To assess if tail fin regeneration is affected when definitive macrophages are ablated, we evaluated tail fin regeneration after amputation by measuring the tail fin area. While primitive macrophage numbers and recruitment were not affected during the regeneration process, definitive macrophages were significantly reduced during the first 48 hpa but recovered by 72 hpa (Figure 4D-G and supplemental Figure 3C-D). We then performed tail fin regeneration analysis and observed no differences in the regenerated tail fin area between larvae treated with either DMSO or MTZ (Figure 4H-I). Our results, thus, indicate that primitive macrophages recruitment to the damage site is not affected and tail fin regeneration is not impaired when definitive macrophages are depleted. Taken together, these data further emphasize that primitive macrophages are sufficient to ensure a timely tissue regeneration and to compensate the absence of other distinct macrophage populations during early developmental stages.

Our study shows that the embryonic hematopoietic system follows a layered strategy to provide a timely supply of innate immune cells and erythrocytes. Under steady-state conditions, we found that the contribution of definitive hematopoietic progenitors to embryonic erythromyeloid lineage is limited. This is of particular interest as none of the

lineage tracing strategies performed in mice, despite their elegant designs, are specific to definitive hematopoietic waves. Our results also complement the recently reported observations that HSCs have a delayed contribution to the lymphomyeloid lineage during development (Ulloa et al., 2021). Together, our observations indicate that the embryonic erythromyeloid lineage is sustained by primitive hematopoietic progenitors under homeostasis.

To investigate the temporal contribution of the macrophage lineage upon tissue injury, we analyzed macrophage recruitment to the damaged tissue during embryonic and early larval developmental stages. We found that primitive macrophages are the only ones recruited to the site of injury during embryonic stages, however, both primitive and definitive macrophage populations were recruited at early larval developmental stages. This difference in recruitment behaviour between primitive and definitive macrophages could be due to that the primitive macrophages are more sensitive to damage sensing and/or a consequence of the immaturity of definitive macrophages at early developmental stages.

Furthermore, as timely recruitment of macrophages to the damage site is important to ensure proper tail fin regeneration (Wynn and Vannella, 2016; Morales and Allende, 2019; Nguyen-Chi et al., 2017; Petrie et al., 2014), we found that the primitive macrophages are the first responders after tail fin injury showed by their earlier recruitment than their definitive counterparts. Thus, we propose that during development, primitive macrophages are more prone to sense signals from the damage site and migrate toward it earlier than their definitive counterparts. These intriguing results suggest that embryos and early larvae adopt a layered ontogeny of macrophages to ensure their abundance for a timely contribution to tissue regeneration.

A major finding of our study is the demonstration that primitive macrophages can solely maintain tissue regeneration during development. This observation was supported by selectively ablating the definitive macrophage pool and analyzing the tail fin area of amputated larvae. We found that the number of recruited primitive macrophages to the site of injury was not altered and tail fin regeneration was not impaired in definitive macrophage-ablated larvae. Together, these results suggest that primitive macrophages are sufficient to ensure tissue regeneration and to compensate the absence of other distinct macrophage populations during critical early developmental stages.

In conclusion, our study provides insights into the ontogeny of the erythromyeloid lineage during embryonic/early larval developmental stages. Our findings support the notion that embryos show a sequential emergence of hematopoietic waves to ensure the abundance of macrophages required for tissue homeostasis and regeneration during a crucial developmental time window. In line with our results, it has been recently reported in mice (Gomez Perdiguero et al., 2015; Patel et al., 2022; Yokomizo et al., 2022; Fanti et al., 2023) and in zebrafish (Tian et al., 2017; Ulloa et al., 2021) that embryonic and adult HSCs do not give rise to several blood subtypes at steady state, upon ablation of mature blood cells, and in response to immune challenge. These observations indicate that ensuring a rapid response to stress to maintain tissue homeostasis in an HSC-independent manner might be a conserved mechanism between species throughout their life.

Materials and Data availability

This study did not generate new unique reagents. The data sets generated during the current study are available from the corresponding authors upon request.

Materials and methods

Zebrafish. Embryonic and adult zebrafish (*Danio rerio*) were maintained at 28°C on a 14-hour light/10 hour dark cycle. The collected embryos were raised in fish water containing 0.01% methylene blue to prevent fungal growth. All fish are housed in the fish facility of our laboratory, which was built according to the local animal welfare standards. All animal procedures were performed in accordance with French and European Union animal welfare guidelines and were evaluated by the ethic committee of the Curie Institute (Paris, France) and approved.

Transgenic lines. The following lines of the AB stain were used: *Tg(fli1a: CreER^{T2})* (Sánchez-Iranzo et al., 2018), *Tg(mpeg1:LoxP-DsRedx-LoxP-GFP-NTR)*(Lin et al., 2019),*Tg(coro1a:loxP-DsRedx-loxP-GFP)* (Xu et al., 2015), *Tg(globin:loxP-DsRedx-loxP-GFP)* (Tian et al., 2017) and *Tg(lck:loxP-DsRedx-loxP-GFP)* (Tian et al., 2017).

Fluorescence Microscopy. Zebrafish embryos, larvae and adults were anesthetized with 0.01% tricaine (A5040, Sigma) and mounted in 2.5% 2.5% methylcellulose in 35-mm imaging dishes (MatTek) as described previously (Renaud et al., 2011). Fluorescent imaging was performed with either Zeiss Axio Zoom V.16 upright microscope with an AxioCam HRm Zeiss camera and Zeiss Zen 3.3 software or with Leica thunder imaging system with Leica LAS-X software. Fluorescence was detected with dsRed and green fluorescent protein (GFP) filters.

Image Analysis. All images were analyzed using FIJI software (Schindelin et al., 2012).

CreER-loxP Cell Labelling (Lineage Tracing). Zebrafish embryos at 24 hpf were treated with 5 µM 4-OHT (H7904, Sigma) for 24 hours. Controls were incubated in the equivalent amount of Ethanol solution during the same period. Light exposure was avoided by using foil to cover the plates as 4-OHT is light sensitive. After treatment, embryos were washed with fresh embryo medium and placed back in incubator. From 5 dpf, larvae were transferred to the fish facility nursery where they were kept and fed. Embryos were raised for further analysis at different developmental stages.

Metronidazole treatment and cell ablation. The *Tg(fli1CreER^{T2};mpeg1:loxP-DsRedx-loxP-GFP-NTR)* embryos were immersed in system water containing 10 mM metronidazole (M1547, Sigma) for 48 hours, which caused an acute depletion of GFP-NTR^{+} cells. The medium containing the MTZ was changed every 24 hours. Controls were incubated in the equivalent amount of DMSO solution during the same period. Light exposure was avoided by using foil to cover the plates as MTZ is light sensitive. Zebrafish were further analyzed by fluorescence imaging at different developmental time points.

Tail Fin Amputation. 2 and 5 dpf larvae were anesthetized with 0.01% tricaine and amputated with a sterile scalpel. The transection was performed by using the posterior section of the

ventral pigmentation gap in the tail fin as a reference, and immediately after amputation larvae were incubated in either E3 medium, or in MTZ in case of macrophage ablation at 28°C.

Quantification of Tail Fin Regeneration. At 24, 48 and 72 hours post amputation or dpa (6,7- and 8-days post fertilization, respectively), larvae were mounted in 2.5% methylcellulose, and regenerating tail fins were imaged in bright field. Tail fin area was measured from the anterior section of the ventral tail fin gap to the end of the regenerating fin, as previously described(Pei et al., 2016), using FiJi software. Tail fin areas were calculated and expressed in square micrometers (um^2).

Quantification of Tail Macrophages. Macrophages were quantified based on their location in the tail (periphery vs CHT) (Figure 2B) in non-amputated larvae. In amputated larvae, recruited macrophages to the site of injury were quantified. Normalization of recruited macrophage numbers was obtained by dividing the number of recruited macrophage subpopulation by their total number in the tail of the same larvae (periphery, CHT and recruited macrophages) (Morales and Allende, 2019).

Quantification and statistical analysis. Statistical analyses were performed by the GraphPad Prism software (Prism 9). All experiments with only two groups and one dependent variable were compared using an unpaired t-test with Welch's correction. Two-way ANOVA with Tukey's multiple comparison was used for this analysis. Statistical data show mean ± s.e.m. Each dot plot value represents an independent embryo, and every experiment was conducted three times independently. The corrected total cell fluorescence (CTCF) was calculated using the formula 'Integrated density whole – (area whole embryo x mean fluorescence background)'. This formula is loosely based on a method described for calculating cell-fluorescence (Ulloa et al., 2021).

Acknowledgments

We thank the Developmental Biology Curie imaging facility (PICT-IBiSA@BDD, Paris, France, UMR3215/U934) members of the France-BioImaging national research infrastructure for their help and advice. We also thank the members of the animal facility of Institut Curie for zebrafish care. We also thank Yohanns Bellaiche, Yazan Salloum and all the members of the Hernandez lab for thoughtful and valuable discussions. We are grateful to Nadia Mercader for providing the *Tg(fli1a:CreERT2)*, we also thank Zilong Wen for providing all the immune and blood lineage switch lines used in this study. This work was supported by the Institut Curie, INSERM, CNRS, the Ville de Paris emergence program (2020 DAE 78), FRM amorçage (AJE201905008718), ATIP-Avenir starting grant R21045DS and the Laboratoire d'Excellence (Labex) DEEP (ANR-11- LBX-0044, ANR-10-IDEX- 0001-02 PSL). R.E. was supported by the Springboard postdoctoral fellowship form Institut Curie and Labex DEEP.

Authors contribution

Conceptualization: R.E. and P.P.H.; Methodology and data collection: R.E., A.M., P.D. and G.G.; Writing - Original Draft: R.E.; Writing - Review & Editing: R.E. and P.P.H.; Funding Acquisition: P.P.H.

Conflict of Interest

The authors declare no competing interests.

References

Bertrand, J.Y., N.C. Chi, B. Santoso, S. Teng, D.Y.R. Stainier, and D. Traver. 2010. Haematopoietic stem cells derive directly from aortic endothelium during development. *Nature*. 464:108–111. doi:10.1038/nature08738.

Bertrand, J.Y., A. Jalil, M. Klaine, S. Jung, A. Cumano, and I. Godin. 2005. Three pathways to mature macrophages in the early mouse yolk sac. *Blood*. 106:3004–3011. doi:10.1182/blood-2005-02-0461.

Bertrand, J.Y., A.D. Kim, E.P. Violette, D.L. Stachura, J.L. Cisson, and D. Traver. 2007. Definitive hematopoiesis initiates through a committed erythromyeloid progenitor in the zebrafish embryo. *Development*. 134:4147–4156. doi:10.1242/dev.012385.

Boisset, J.-C., W. van Cappellen, C. Andrieu-Soler, N. Galjart, E. Dzierzak, and C. Robin. 2010. In vivo imaging of haematopoietic cells emerging from the mouse aortic endothelium. *Nature*. 464:116–120. doi:10.1038/nature08764.

Busch, K., K. Klapproth, M. Barile, M. Flossdorf, T. Holland-Letz, S.M. Schlenner, M. Reth, T. Höfer, and H.-R. Rodewald. 2015. Fundamental properties of unperturbed haematopoiesis from stem cells in vivo. *Nature*. 518:542–546. doi:10.1038/nature14242.

Carney, T.J., and C. Mosimann. 2018. Switch and Trace: Recombinase Genetics in Zebrafish. *Trends Genet*. 34:362–378. doi:10.1016/j.tig.2018.01.004.

Cumano, A., F. Dieterlen-Lievre, and I. Godin. 1996. Lymphoid potential, probed before circulation in mouse, is restricted to caudal intraembryonic splanchnopleura. *Cell*. 86:907–916. doi:10.1016/s0092-8674(00)80166-x.

Curado, S., D.Y.R. Stainier, and R.M. Anderson. 2008. Nitroreductase-mediated cell/tissue ablation in zebrafish: a spatially and temporally controlled ablation method with applications in developmental and regeneration studies. *Nat Protoc*. 3:948–954. doi:10.1038/nprot.2008.58.

Ebisuya, M., and J. Briscoe. 2018. What does time mean in development? *Development*. 145:dev164368. doi:10.1242/dev.164368.

Ellett, F., L. Pase, J.W. Hayman, A. Andrianopoulos, and G.J. Lieschke. 2011. mpeg1 promoter transgenes direct macrophage-lineage expression in zebrafish. *Blood*. 117:e49–e56. doi:10.1182/blood-2010-10-314120.

Elsaid, R., S. Meunier, O. Burlen-Defranoux, F. Soares-da-Silva, T. Perchet, L. Iturri, L. Freyer, P. Vieira, P. Pereira, R. Golub, A. Bandeira, E.G. Perdiguero, and A. Cumano. 2021. A wave of bipotent T/ILC-restricted progenitors shapes the embryonic thymus

472 microenvironment in a time-dependent manner. *Blood*. 137:1024–1036.
473 doi:10.1182/blood.2020006779.

474 Elsaid, R., F. Soares-da-Silva, M. Peixoto, D. Amiri, N. Mackowski, P. Pereira, A. Bandeira, and
475 A. Cumano. 2020. Hematopoiesis: A Layered Organization Across Chordate Species.
476 *Front. Cell Dev. Biol.* 8:606642. doi:10.3389/fcell.2020.606642.

477 Fanti, A.-K., K. Busch, A. Greco, X. Wang, B. Cirovic, F. Shang, T. Nizharadze, L. Frank, M.
478 Barile, T.B. Feyerabend, T. Höfer, and H.-R. Rodewald. 2023. Flt3- and Tie2-Cre
479 tracing identifies regeneration in sepsis from multipotent progenitors but not
480 hematopoietic stem cells. *Cell Stem Cell*. 0. doi:10.1016/j.stem.2022.12.014.

481 Ferrero, G., C.B. Mahony, E. Dupuis, L. Yvernogeau, E. Di Ruggiero, M. Miserocchi, M. Caron,
482 C. Robin, D. Traver, J.Y. Bertrand, and V. Wittamer. 2018. Embryonic Microglia Derive
483 from Primitive Macrophages and Are Replaced by cmyb-Dependent Definitive
484 Microglia in Zebrafish. *Cell Reports*. 24:130–141. doi:10.1016/j.celrep.2018.05.066.

485 Frame, J.M., K.H. Fegan, S.J. Conway, K.E. McGrath, and J. Palis. 2016. Definitive
486 Hematopoiesis in the Yolk Sac Emerges from Wnt-Responsive Hemogenic
487 Endothelium Independently of Circulation and Arterial Identity. *Stem Cells*. 34:431–
488 444. doi:10.1002/stem.2213.

489 Ganis, J.J., N. Hsia, E. Trompouki, J.L.O. de Jong, A. DiBiase, J.S. Lambert, Z. Jia, P.J. Sabo, M.
490 Weaver, R. Sandstrom, J.A. Stamatoyannopoulos, Y. Zhou, and L.I. Zon. 2012.
491 Zebrafish globin Switching Occurs in Two Developmental Stages and is Controlled by
492 the LCR. *Dev Biol*. 366:185–194. doi:10.1016/j.ydbio.2012.03.021.

493 Gentek, R., C. Ghigo, G. Hoeffel, M.J. Bulle, R. Msallam, G. Gautier, P. Launay, J. Chen, F.
494 Ginhoux, and M. Bajénoff. 2018. Hemogenic Endothelial Fate Mapping Reveals Dual
495 Developmental Origin of Mast Cells. *Immunity*. 48:1160-1171.e5.
496 doi:10.1016/j.immuni.2018.04.025.

497 Gomez Perdiguero, E., K. Klapproth, C. Schulz, K. Busch, E. Azzoni, L. Crozet, H. Garner, C.
498 Trouillet, M.F. de Bruijn, F. Geissmann, and H.-R. Rodewald. 2015. Tissue-resident
499 macrophages originate from yolk-sac-derived erythro-myeloid progenitors. *Nature*.
500 518:547–551. doi:10.1038/nature13989.

501 He, S., J. Chen, Y. Jiang, Y. Wu, L. Zhu, W. Jin, C. Zhao, T. Yu, T. Wang, S. Wu, X. Lin, J.Y. Qu, Z.
502 Wen, W. Zhang, and J. Xu. 2018. Adult zebrafish Langerhans cells arise from
503 hematopoietic stem/progenitor cells. *eLife*. 7:e36131. doi:10.7554/eLife.36131.

504 Henninger, J., B. Santoso, S. Hans, E. Durand, J. Moore, C. Mosimann, M. Brand, D. Traver,
505 and L. Zon. 2017. Clonal fate mapping quantifies the number of haematopoietic stem
506 cells that arise during development. *Nat Cell Biol*. 19:17–27. doi:10.1038/ncb3444.

507 Herbomel, P., B. Thisse, and C. Thisse. 2001. Zebrafish Early Macrophages Colonize Cephalic
508 Mesenchyme and Developing Brain, Retina, and Epidermis through a M-CSF
509 Receptor-Dependent Invasive Process. *Developmental Biology*. 238:274–288.
510 doi:10.1006/dbio.2001.0393.

Hoeffel, G., J. Chen, Y. Lavin, D. Low, F.F. Almeida, P. See, A.E. Beaudin, J. Lum, I. Low, E.C. Forsberg, M. Poidinger, F. Zolezzi, A. Larbi, L.G. Ng, J.K.Y. Chan, M. Greter, B. Becher, I.M. Samokhvalov, M. Merad, and F. Ginhoux. 2015. C-Myb(+) erythro-myeloid progenitor-derived fetal monocytes give rise to adult tissue-resident macrophages. *Immunity*. 42:665–678. doi:10.1016/j.immuni.2015.03.011.

Kingsley, P.D., J. Malik, K.A. Fantauzzo, and J. Palis. 2004. Yolk sac-derived primitive erythroblasts enucleate during mammalian embryogenesis. *Blood*. 104:19–25. doi:10.1182/blood-2003-12-4162.

Kissa, K., and P. Herbomel. 2010a. Blood stem cells emerge from aortic endothelium by a novel type of cell transition. *Nature*. 464:112–115. doi:10.1038/nature08761.

Kissa, K., and P. Herbomel. 2010b. Blood stem cells emerge from aortic endothelium by a novel type of cell transition. *Nature*. 464:112–115. doi:10.1038/nature08761.

Langenau, D.M., A.A. Ferrando, D. Traver, J.L. Kutok, J.-P.D. Hezel, J.P. Kanki, L.I. Zon, A.T. Look, and N.S. Trede. 2004. In vivo tracking of T cell development, ablation, and engraftment in transgenic zebrafish. *Proc Natl Acad Sci U S A*. 101:7369–7374. doi:10.1073/pnas.0402248101.

Li, L., B. Yan, Y.-Q. Shi, W.-Q. Zhang, and Z.-L. Wen. 2012. Live Imaging Reveals Differing Roles of Macrophages and Neutrophils during Zebrafish Tail Fin Regeneration. *J Biol Chem*. 287:25353–25360. doi:10.1074/jbc.M112.349126.

Lin, X., Q. Zhou, C. Zhao, G. Lin, J. Xu, and Z. Wen. 2019. An Ectoderm-Derived Myeloid-like Cell Population Functions as Antigen Transporters for Langerhans Cells in Zebrafish Epidermis. *Developmental Cell*. 49:605-617.e5. doi:10.1016/j.devcel.2019.03.028.

McGrath, K.E., J.M. Frame, K.H. Fegan, J.R. Bowen, S.J. Conway, S.C. Catherman, P.D. Kingsley, A.D. Koniski, and J. Palis. 2015a. Distinct Sources of Hematopoietic Progenitors Emerge before HSCs and Provide Functional Blood Cells in the Mammalian Embryo. *Cell Rep*. 11:1892–1904. doi:10.1016/j.celrep.2015.05.036.

McGrath, K.E., J.M. Frame, and J. Palis. 2015b. Early hematopoiesis and macrophage development. *Semin Immunol*. 27:379–387. doi:10.1016/j.smim.2016.03.013.

Medvinsky, A., and E. Dzierzak. 1996. Definitive hematopoiesis is autonomously initiated by the AGM region. *Cell*. 86:897–906. doi:10.1016/s0092-8674(00)80165-8.

Morales, R.A., and M.L. Allende. 2019. Peripheral Macrophages Promote Tissue Regeneration in Zebrafish by Fine-Tuning the Inflammatory Response. *Front. Immunol.* 10:253. doi:10.3389/fimmu.2019.00253.

Murayama, E., K. Kissa, A. Zapata, E. Mordelet, V. Briolat, H.-F. Lin, R.I. Handin, and P. Herbomel. 2006. Tracing hematopoietic precursor migration to successive hematopoietic organs during zebrafish development. *Immunity*. 25:963–975. doi:10.1016/j.immuni.2006.10.015.

548 Nguyen-Chi, M., B. Laplace-Builhé, J. Travnickova, P. Luz-Crawford, G. Tejedor, G. Lutfalla, K.
549 Kissa, C. Jorgensen, and F. Djouad. 2017. TNF signaling and macrophages govern fin
550 regeneration in zebrafish larvae. *Cell Death Dis*. 8:e2979–e2979.
551 doi:10.1038/cddis.2017.374.

552 Palis, J. 2014. Primitive and definitive erythropoiesis in mammals. *Frontiers in Physiology*. 5.

553 Palis, J., R.J. Chan, A. Koniski, R. Patel, M. Starr, and M.C. Yoder. 2001. Spatial and temporal
554 emergence of high proliferative potential hematopoietic precursors during murine
555 embryogenesis. *Proc Natl Acad Sci U S A*. 98:4528–4533.
556 doi:10.1073/pnas.071002398.

557 Palis, J., S. Robertson, M. Kennedy, C. Wall, and G. Keller. 1999. Development of erythroid
558 and myeloid progenitors in the yolk sac and embryo proper of the mouse.
559 *Development*. 126:5073–5084. doi:10.1242/dev.126.22.5073.

560 Patel, S.H., C. Christodoulou, C. Weinreb, Q. Yu, E.L. da Rocha, B.J. Pepe-Mooney, S. Bowling,
561 L. Li, F.G. Osorio, G.Q. Daley, and F.D. Camargo. 2022. Lifelong multilineage
562 contribution by embryonic-born blood progenitors. *Nature*. 606:747–753.
563 doi:10.1038/s41586-022-04804-z.

564 Pei, W., K. Tanaka, S.C. Huang, L. Xu, B. Liu, J. Sinclair, J. Idol, G.K. Varshney, H. Huang, S. Lin,
565 R.B. Nussenblatt, R. Mori, and S.M. Burgess. 2016. Extracellular HSP60 triggers tissue
566 regeneration and wound healing by regulating inflammation and cell proliferation.
567 *npj Regen Med*. 1:1–11. doi:10.1038/npjregenmed.2016.13.

568 Petrie, T.A., N.S. Strand, C. Tsung-Yang, J.S. Rabinowitz, and R.T. Moon. 2014. Macrophages
569 modulate adult zebrafish tail fin regeneration. *Development*. 141:2581–2591.
570 doi:10.1242/dev.098459.

571 Renaud, O., P. Herbomel, and K. Kissa. 2011. Studying cell behavior in whole zebrafish
572 embryos by confocal live imaging: application to hematopoietic stem cells. *Nat*
573 *Protoc*. 6:1897–1904. doi:10.1038/nprot.2011.408.

574 Sánchez-Iranzo, H., M. Galardi-Castilla, A. Sanz-Morejón, J.M. González-Rosa, R. Costa, A.
575 Ernst, J. Sainz de Aja, X. Langa, and N. Mercader. 2018. Transient fibrosis resolves via
576 fibroblast inactivation in the regenerating zebrafish heart. *Proc. Natl. Acad. Sci.*
577 *U.S.A.* 115:4188–4193. doi:10.1073/pnas.1716713115.

578 Schindelin, J., I. Arganda-Carreras, E. Frise, V. Kaynig, M. Longair, T. Pietzsch, S. Preibisch, C.
579 Rueden, S. Saalfeld, B. Schmid, J.-Y. Tinevez, D.J. White, V. Hartenstein, K. Eliceiri, P.
580 Tomancak, and A. Cardona. 2012. Fiji: an open-source platform for biological-image
581 analysis. *Nat Methods*. 9:676–682. doi:10.1038/nmeth.2019.

582 Soares-da-Silva, F., L. Freyer, R. Elsaid, O. Burlen-Defranoux, L. Iturri, O. Sismeiro, P. Pinto-
583 do-Ó, E. Gomez-Perdiguero, and A. Cumano. 2021. Yolk sac, but not hematopoietic
584 stem cell-derived progenitors, sustain erythropoiesis throughout murine embryonic
585 life. *J Exp Med*. 218:e20201729. doi:10.1084/jem.20201729.

586 Stachura, D.L., and D. Traver. 2011. Chapter 4 - Cellular Dissection of Zebrafish
587 Hematopoiesis. *In* Methods in Cell Biology. H.W. Detrich, M. Westerfield, and L.I.
588 Zon, editors. Academic Press. 75–110.

589 Tian, Y., J. Xu, S. Feng, S. He, S. Zhao, L. Zhu, W. Jin, Y. Dai, L. Luo, J.Y. Qu, and Z. Wen. 2017.
590 The first wave of T lymphopoiesis in zebrafish arises from aorta endothelium
591 independent of hematopoietic stem cells. *Journal of Experimental Medicine*.
592 214:3347–3360. doi:10.1084/jem.20170488.

593 Ulloa, B.A., S.S. Habbsa, K.S. Potts, A. Lewis, M. McKinstry, S.G. Payne, J.C. Flores, A. Nizhnik,
594 M. Feliz Norberto, C. Mosimann, and T.V. Bowman. 2021. Definitive hematopoietic
595 stem cells minimally contribute to embryonic hematopoiesis. *Cell Reports*.
596 36:109703. doi:10.1016/j.celrep.2021.109703.

597 Wynn, T.A., and K.M. Vannella. 2016. Macrophages in Tissue Repair, Regeneration, and
598 Fibrosis. *Immunity*. 44:450–462. doi:10.1016/j.immuni.2016.02.015.

599 Xu, J., L. Zhu, S. He, Y. Wu, W. Jin, T. Yu, J.Y. Qu, and Z. Wen. 2015. Temporal-Spatial
600 Resolution Fate Mapping Reveals Distinct Origins for Embryonic and Adult Microglia
601 in Zebrafish. *Developmental Cell*. 34:632–641. doi:10.1016/j.devcel.2015.08.018.

602 Yokomizo, T., T. Ideue, S. Morino-Koga, C.Y. Tham, T. Sato, N. Takeda, Y. Kubota, M.
603 Kurokawa, N. Komatsu, M. Ogawa, K. Araki, M. Osato, and T. Suda. 2022.
604 Independent origins of fetal liver haematopoietic stem and progenitor cells. *Nature*.
605 609:779–784. doi:10.1038/s41586-022-05203-0.

606

Graphical abstract

Steady state

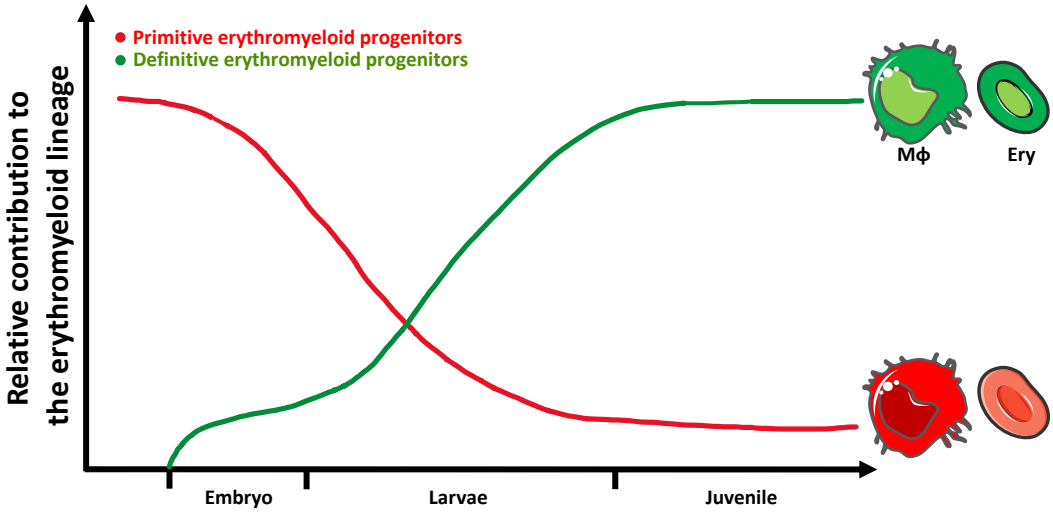

Caudal fin Injury

During embryonic stages

During early larval developmental stages

During early larval developmental stages upon ablation of definitive macrophages

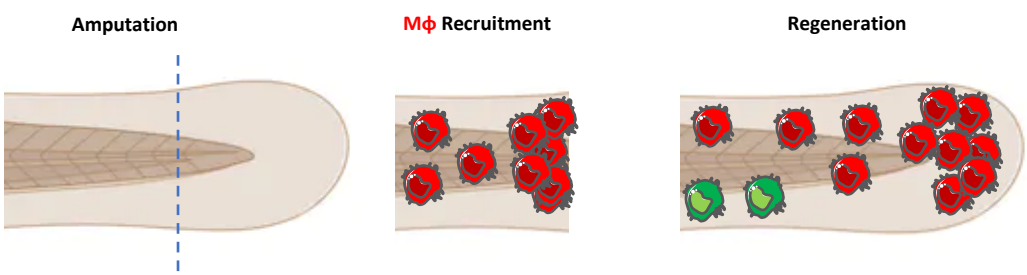

Figure 1

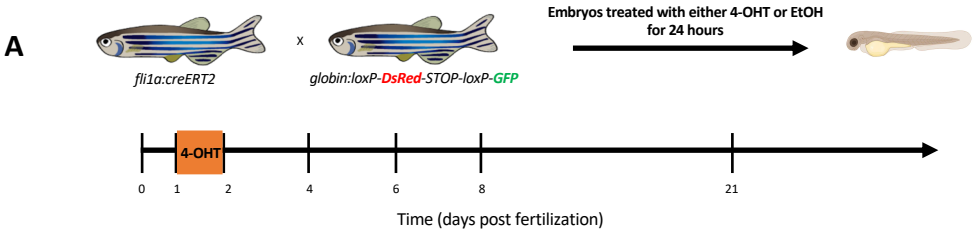
A
fli1a:creERT2
x
globin:loxP-DsRed-STOP-loxP-GFP
Embryos treated with either 4-OHT or EtOH
for 24 hours
4-OHT
0
1
2
4
6
8
21
Time (days post fertilization)

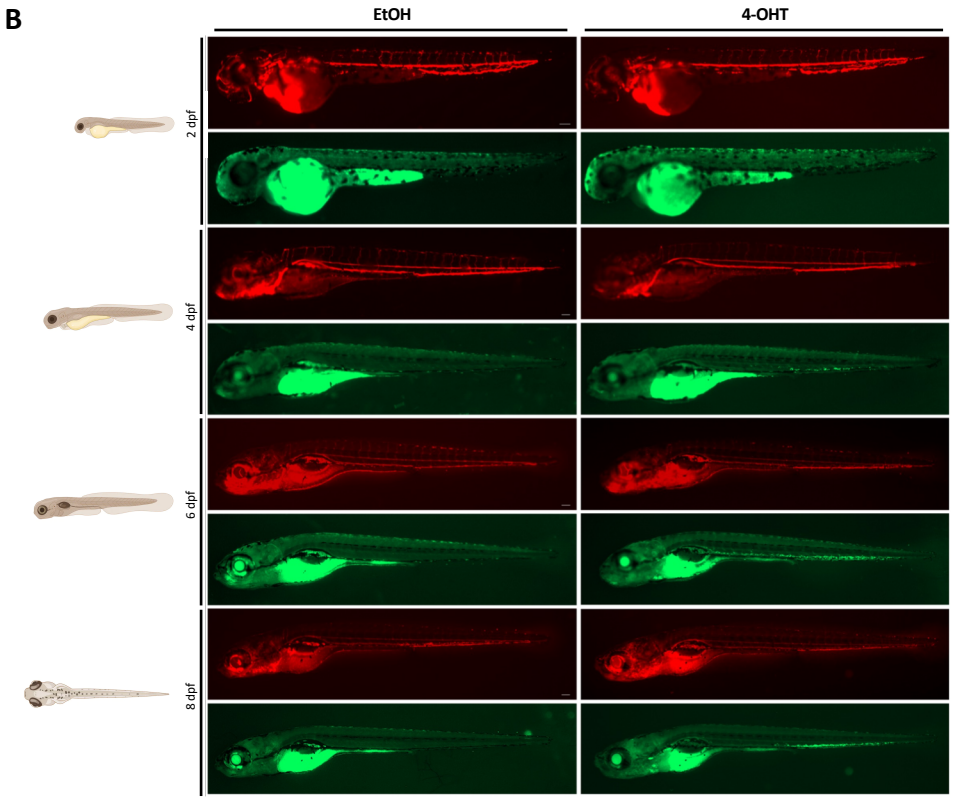
B
EtOH
4-OHT
2 dpf
4 dpf
6 dpf
8 dpf

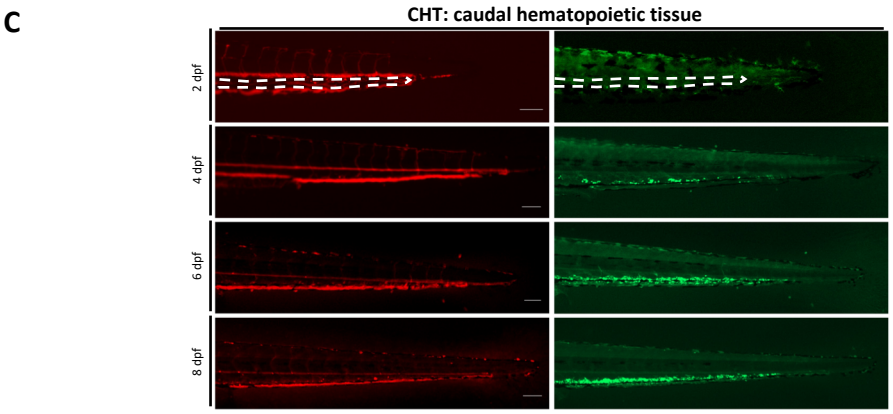
C
CHT: caudal hematopoietic tissue
2 dpf
4 dpf
6 dpf
8 dpf

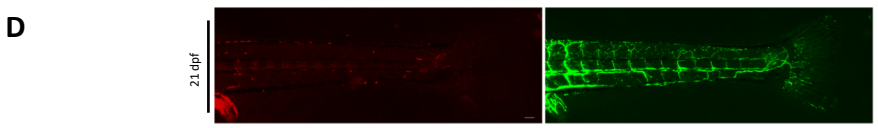
D
21 dpf

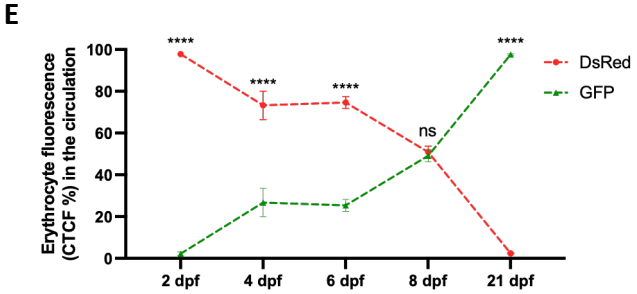
E
Erythrocyte fluorescence (CTCF %) in the circulation
100
80
60
40
20
0
****
****
****
ns
****
2 dpf
4 dpf
6 dpf
8 dpf
21 dpf
DsRed
GFP

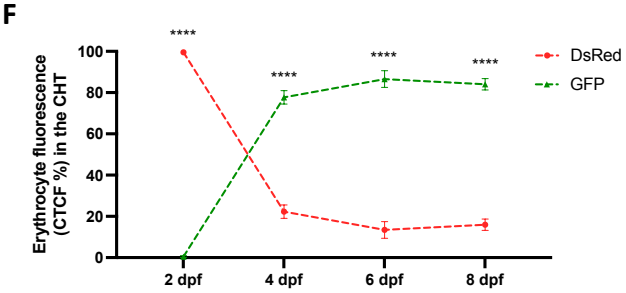
F
Erythrocyte fluorescence (CTCF %) in the CHT
100
80
60
40
20
0
****
****
****
****
2 dpf
4 dpf
6 dpf
8 dpf
DsRed
GFP

Figure 2

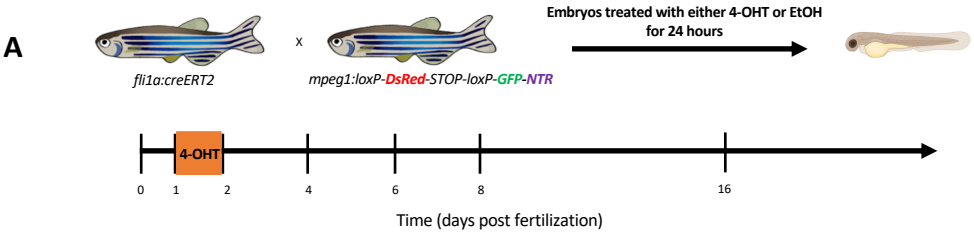
A
fli1a:creERT2
X
mpeg1:loxP-DsRed-STOP-loxP-GFP-NTR
Embryos treated with either 4-OHT or EtOH
for 24 hours
4-OHT
0
1
2
4
6
8
16
Time (days post fertilization)

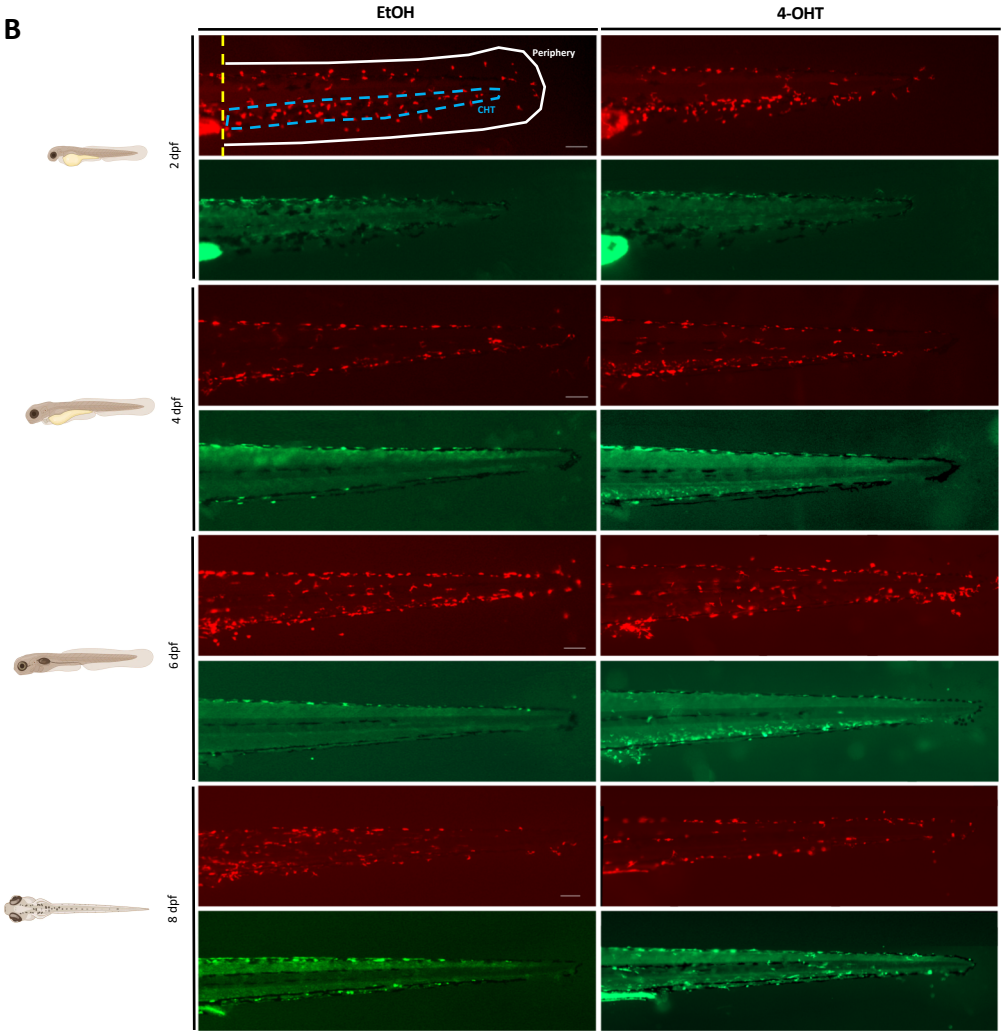
B
EtOH
4-OHT
Periphery
CHT
2 dpf
4 dpf
6 dpf
8 dpf

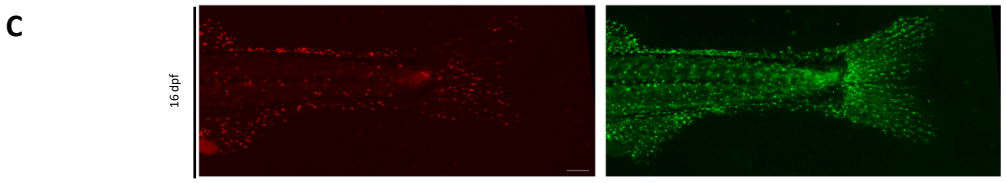
C
16 dpf

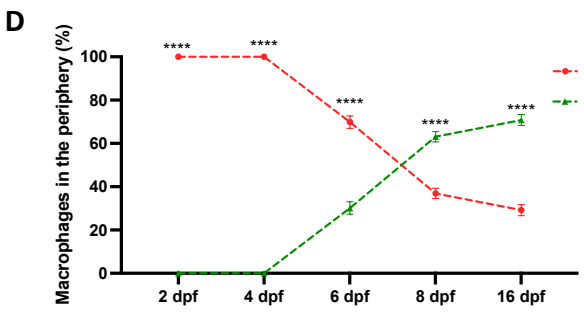
D
Macrophages in the periphery (%)
100
80
60
40
20
0
****
DsRed
GFP
2 dpf
4 dpf
6 dpf
8 dpf
16 dpf

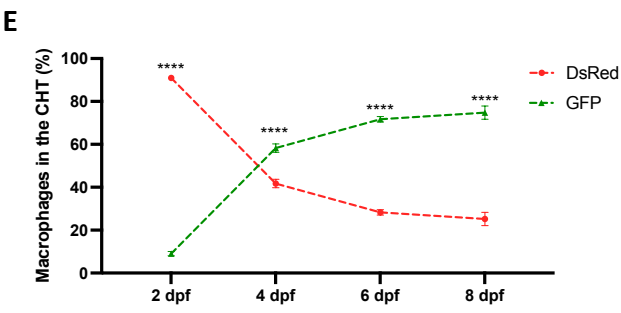
E
Macrophages in the CHT (%)
100
80
60
40
20
0
****
DsRed
GFP
2 dpf
4 dpf
6 dpf
8 dpf

Figure 3

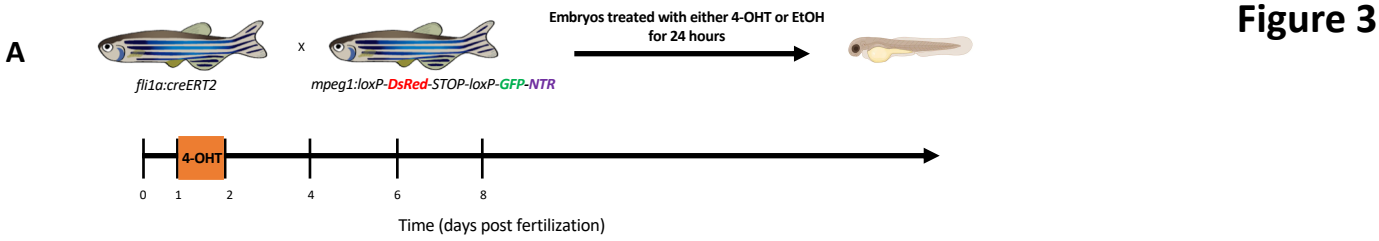
A
fli1a:creERT2
x
mpeg1:loxP-DsRed-STOP-loxP-GFP-NTR
Embryos treated with either 4-OHT or EtOH for 24 hours
4-OHT
0 1 2 4 6 8
Time (days post fertilization)

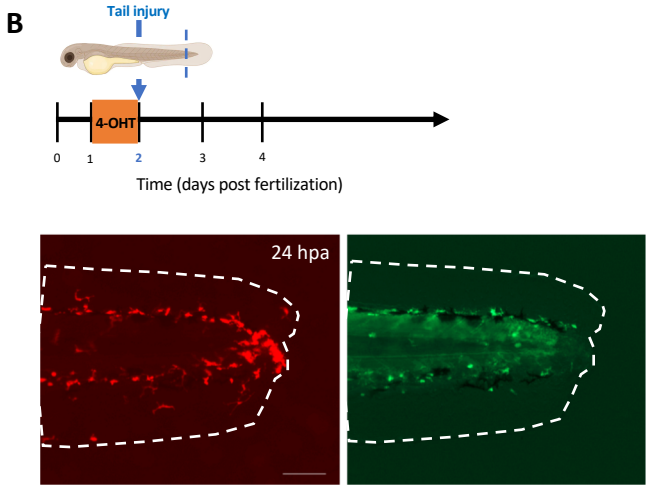
B
Tail injury
4-OHT
0 1 2 3 4
Time (days post fertilization)
24 hpa

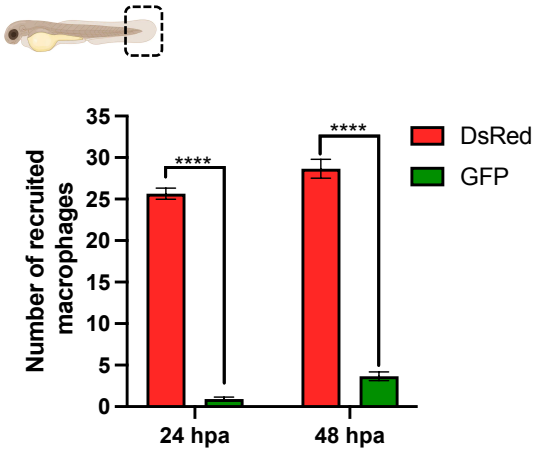
C
Number of recruited macrophages
35
30
25
20
15
10
5
0
****
****
DsRed
GFP
24 hpa
48 hpa

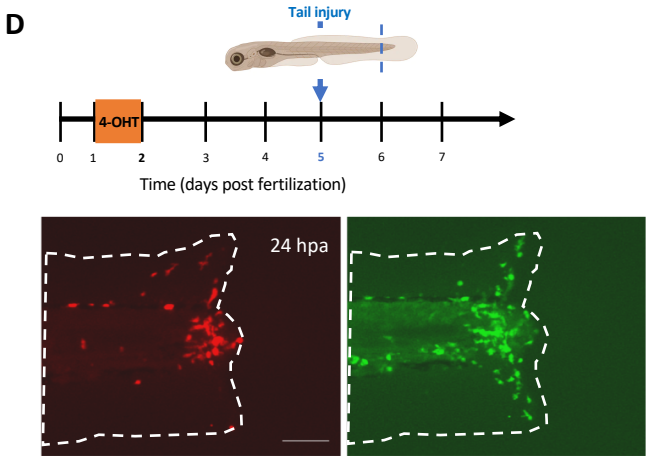
D
Tail injury
4-OHT
0 1 2 3 4 5 6 7
Time (days post fertilization)
24 hpa

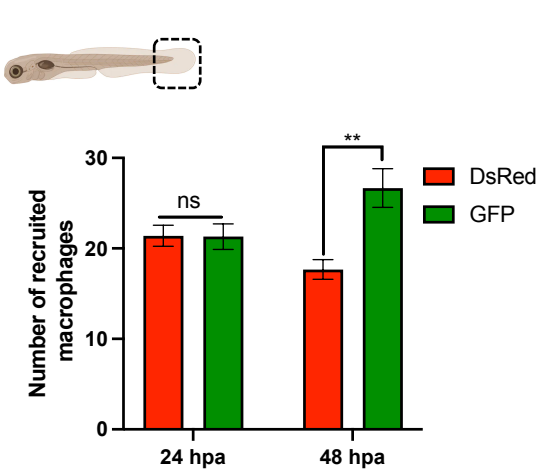
E
Number of recruited macrophages
30
20
10
0
ns
**
DsRed
GFP
24 hpa
48 hpa

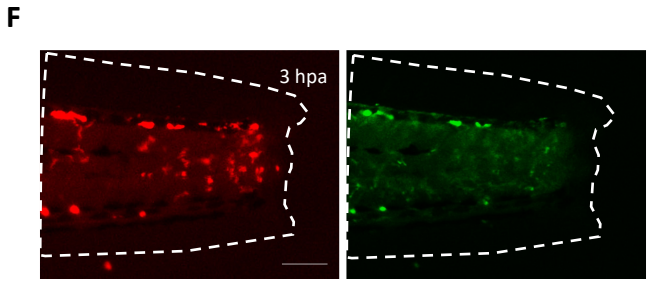
F
3 hpa

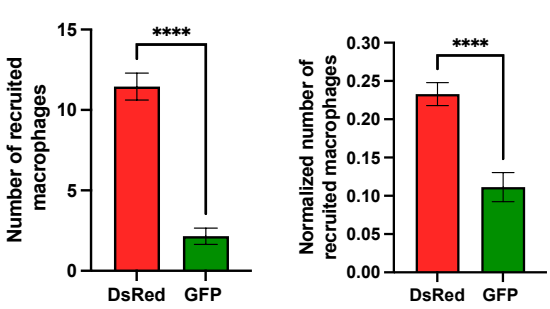
G
Number of recruited macrophages
15
10
5
0
****
DsRed
GFP
Normalized number of recruited macrophages
0.30
0.25
0.20
0.15
0.10
0.05
0.00
****
DsRed
GFP

Figure 4

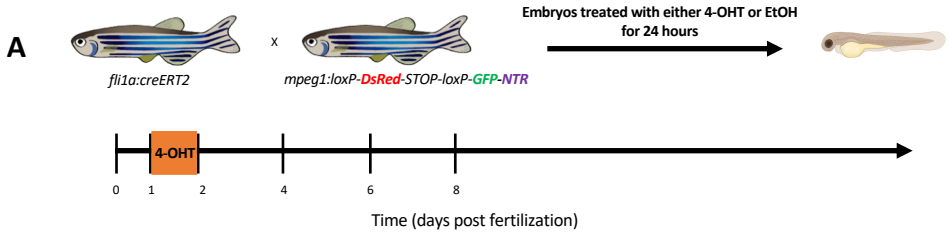
A
fli1a:creERT2
x
mpeg1:loxP-DsRed-STOP-loxP-GFP-NTR
Embryos treated with either 4-OHT or EtOH for 24 hours
4-OHT
0 1 2 4 6 8
Time (days post fertilization)

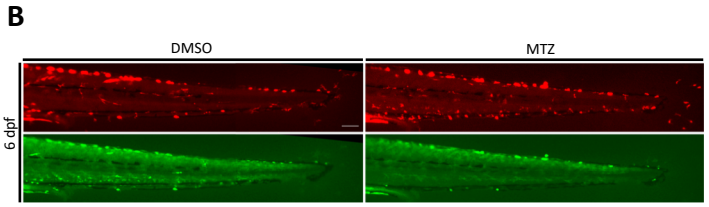
B
DMSO
MTZ
6 dpf

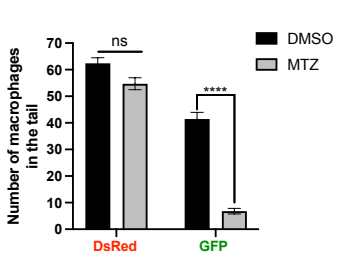
C
Number of macrophages in the tail
ns
****
DMSO
MTZ
DsRed
GFP

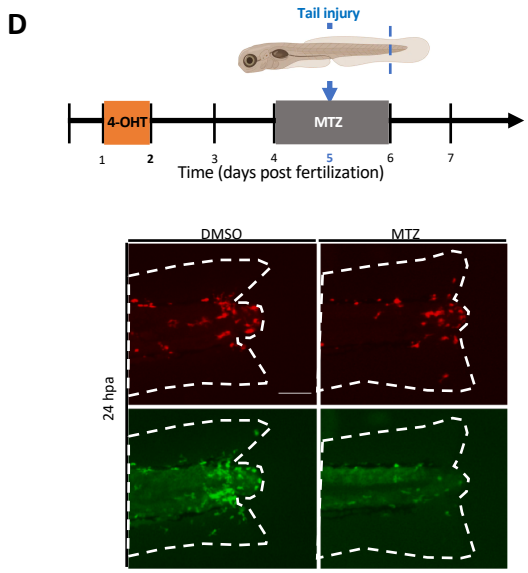
D
Tail injury
4-OHT
MTZ
1 2 3 4 5 6 7
Time (days post fertilization)
DMSO
MTZ
24 hpa

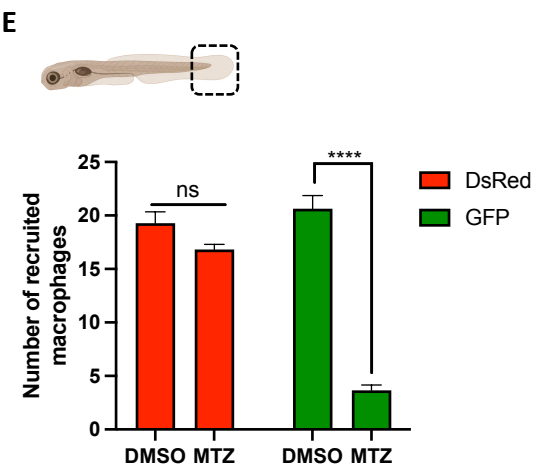
E
Number of recruited macrophages
ns
****
DsRed
GFP
DMSO MTZ
DMSO MTZ

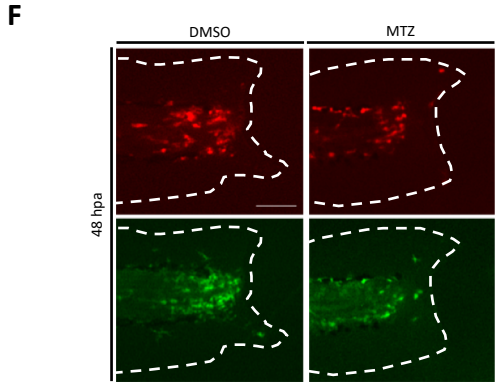
F
DMSO
MTZ
48 hpa

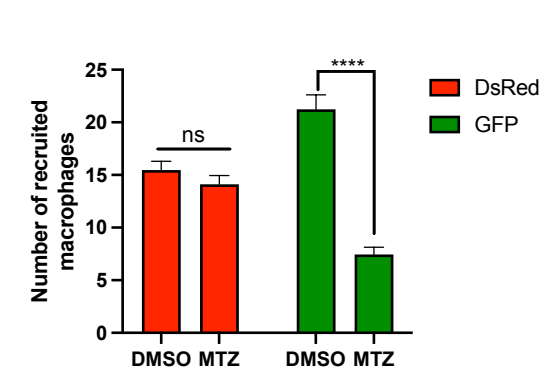
G
Number of recruited macrophages
ns
****
DsRed
GFP
DMSO MTZ
DMSO MTZ

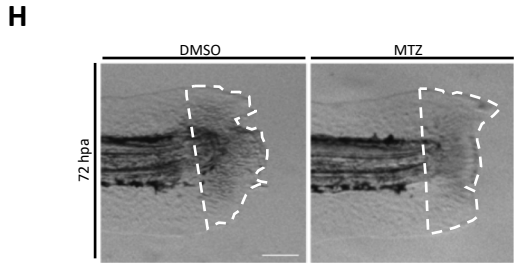
H
DMSO
MTZ
72 hpa

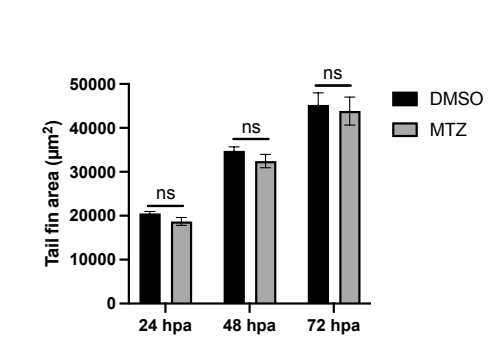
I
Tail fin area (μm²)
ns
ns
ns
DMSO
MTZ
24 hpa
48 hpa
72 hpa

Supp Figure 1

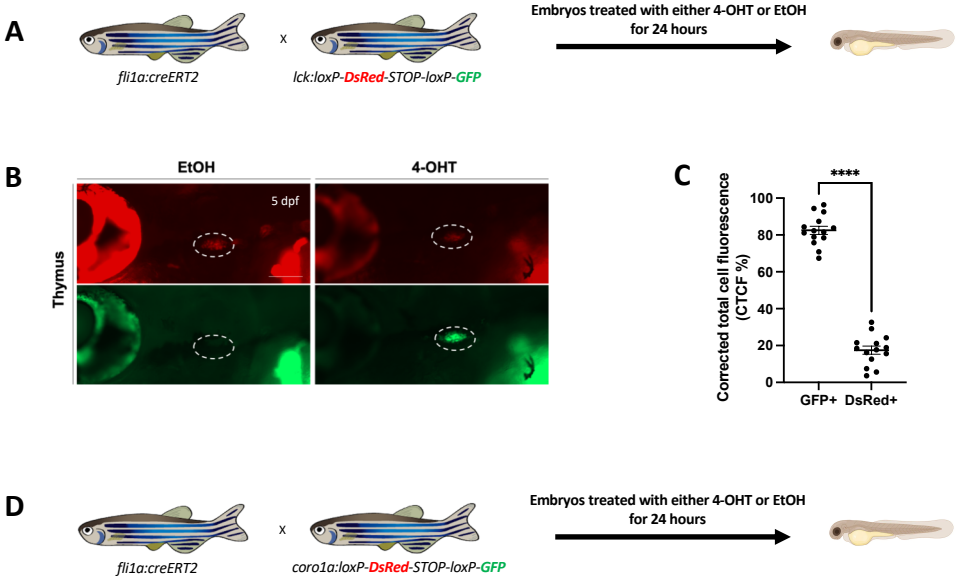

CHT: caudal hematopoietic tissue

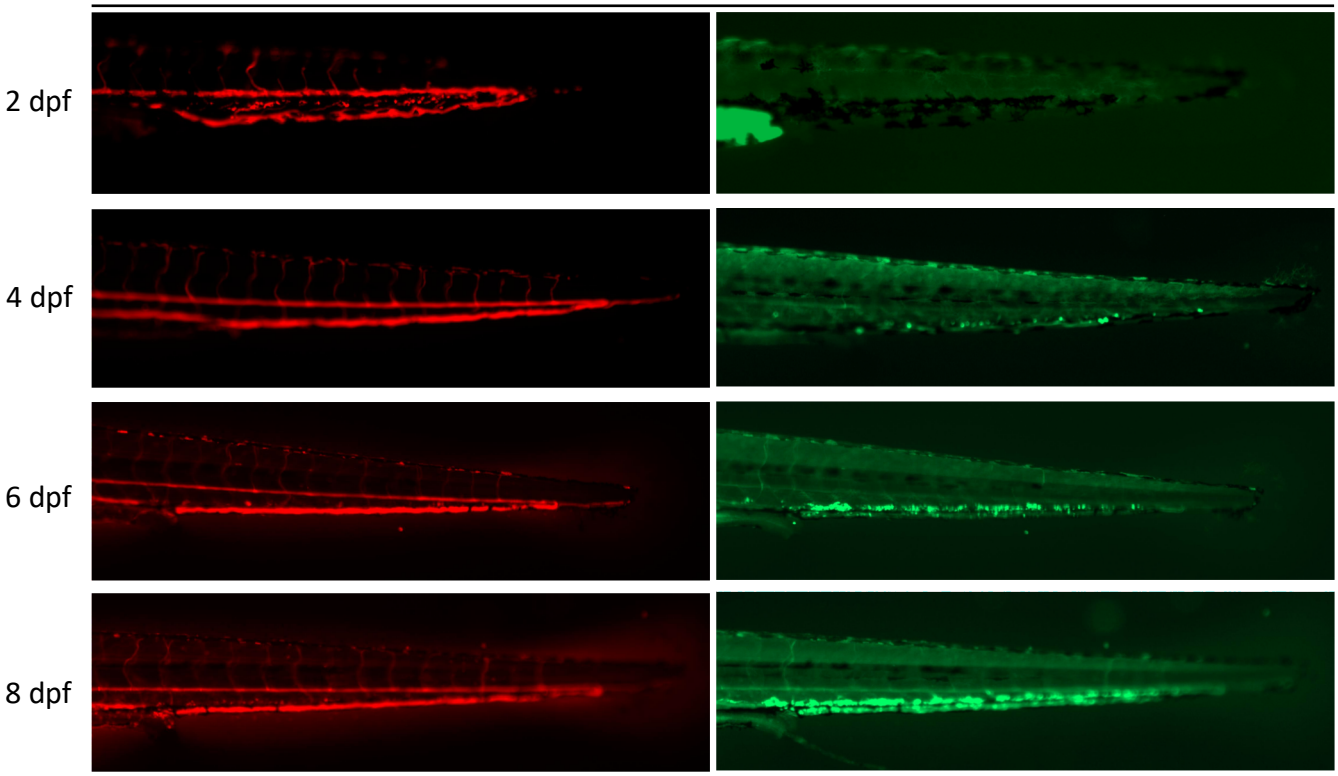

Supp Figure 2.Related to Fig. 2

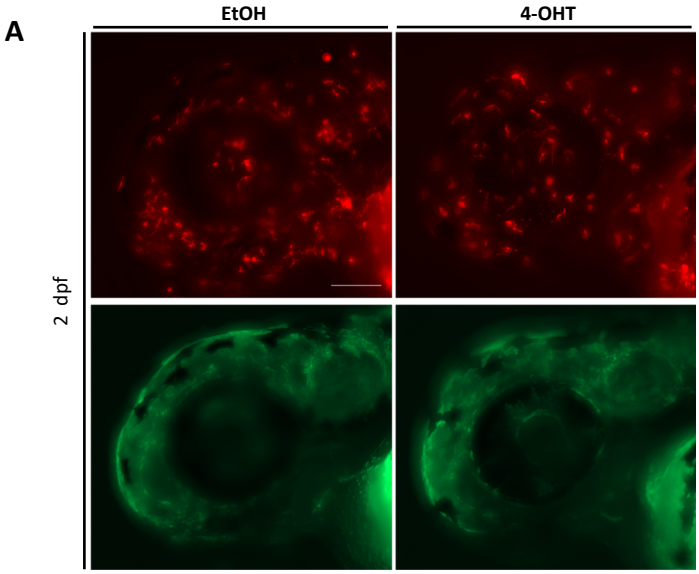

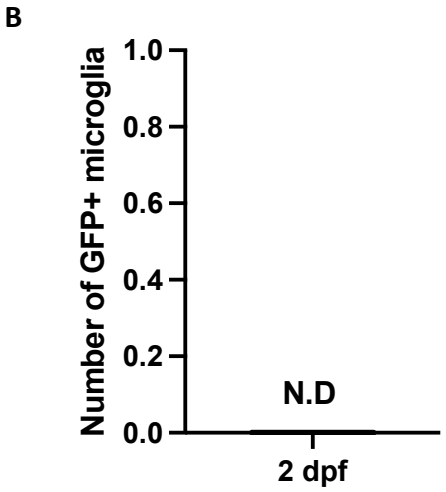

Supp Figure 3. Related to Fig. 3 and 4

A

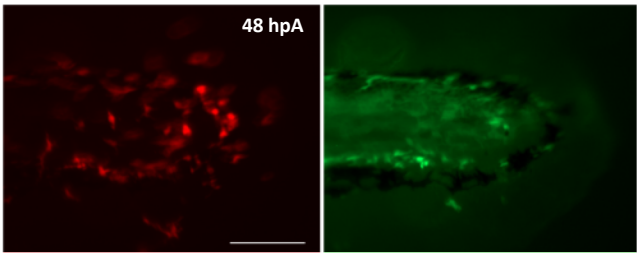

B

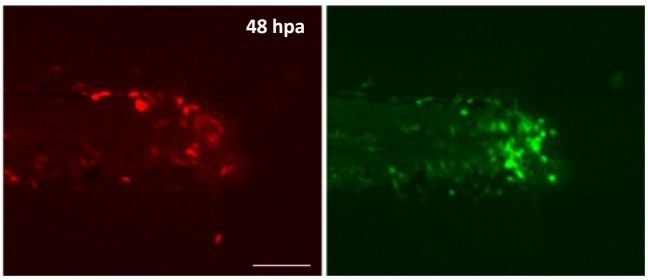

C

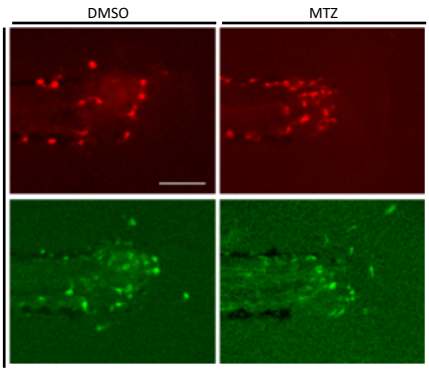

D

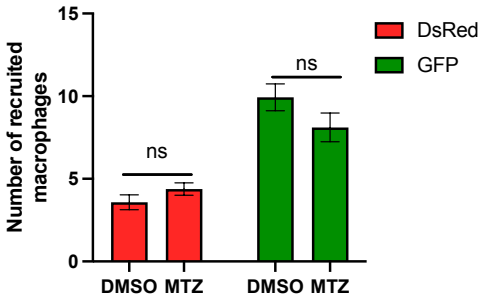

Figure 1: Tracing the contribution of definitive hematopoietic waves to the erythroid lineage in the embryo and early larvae.

(A) Scheme of the 4-OHT-inducible transgenic lines used to assess the contribution of definitive hematopoietic waves to the erythroid lineage.
(B) Fluorescent images of EtOH non-switched controls (right) and 4-OHT-induced (left) *Tg(fli1a:creERT2;globin:Switch)* embryos and larvae (2 dpf-8 dpf). Scale bars, 100 µm. Representative images are shown with quantification of erythrocytes in circulation in (E).
(C) Fluorescent images of 4-OHT-induced *Tg(fli1a:creERT2;globin:Switch)* embryos and larvae (2-8 dpf) in the CHT region. Non-switched primitive erythrocytes (right) and definitive erythrocytes (left). Scale bars, 100 µm. Representative images are shown with quantification of erythrocytes in the CHT in (F).
(D) Fluorescent images of 4-OHT-induced *Tg(fli1a:creERT2;globin:Switch)* (21 dpf) in the circulation. Scale bar, 100 µm. Non-switched primitive erythrocytes (right) and definitive erythrocytes (left). Representative images are shown with quantification of erythrocytes in the circulation in (E).
(E) Quantification of DsRed and GFP fluorescence intensity percentage in the circulation was measured over a time course of 2-21 dpf. (2 dpf n=6; 4 dpf n=4; 6 dpf n=5; 8 dpf n=4; 21 dpf n=5). Mean ± SEM of the $DsRed^+$ and GFP^+ corrected total cell fluorescence (CTCF) percentage at each time point is shown. Two-way ANOVA with Sidak's multiple comparison was used for this analysis. $^{****}p \leq 0.0001$.
(F) Quantification of DsRed and GFP fluorescence intensity percentage in the CHT was measured over a time course of 2-8 dpf. (2 dpf n=6; 4 dpf n=4; 6 dpf n=5; 8 dpf n=4). Mean ± SEM of the $DsRed^+$ and GFP^+ corrected total cell fluorescence (CTCF) percentage at each time point is shown. Two-way ANOVA with Sidak's multiple comparison was used for this analysis. $^{****}p \leq 0.0001$.

Figure 2: Tracing the contribution of definitive hematopoietic waves to macrophages in the embryo and early larvae.

(A) Scheme of the 4-OHT-inducible transgenic lines used to assess the contribution of definitive hematopoietic waves to the macrophage lineage.
(B) Fluorescent images of EtOH non-switched controls (right) and 4-OHT-induced (left) *Tg(fli1a:creERT2;mpeg1:Switch)* embryos and larvae (2 dpf-8 dpf). Macrophages were considered as peripheral macrophages (white area) or CHT-resident macrophages (blue area). Scale bars, 100 µm. Representative images are shown with quantification of macrophages in the periphery in (D) and the CHT in (E).
(C) Fluorescent images of 4-OHT-induced *Tg(fli1a:creERT2;mpeg1:Switch)* (16 dpf) in the periphery. Scale bar, 500 µm. Non-switched primitive macrophages (right) and definitive macrophages (left). Representative images are shown with quantification of macrophages in the periphery in (D).
(D) Quantification of DsRed and GFP macrophage number in the periphery was measured over a time course of 2-16 dpf. (2 dpf n=6; 4 dpf n=11; 6 dpf n=7; 8 dpf n=4; 16 dpf n=3). Mean ± SEM of the $DsRed^+$ and GFP^+ macrophage number at each time point is shown. Two-way ANOVA with Sidak's multiple comparison was used for this analysis. $^{****}p \leq 0.0001$.
(E) Quantification of DsRed and GFP macrophage number in the CHT was measured over a time course of 2-8 dpf. (2 dpf n=6; 4 dpf n=11; 6 dpf n=7; 8 dpf n=4). Mean ± SEM of the $DsRed^+$ and GFP^+ macrophage number at each time point is shown. Two-way ANOVA with Sidak's multiple comparison was used for this analysis. $^{****}p \leq 0.0001$.

Figure 3: Ontogenetically distinct macrophages exhibit different migration behavior and recruitment after tissue injury during early developmental stages.

(A) Scheme of the 4-OHT-inducible transgenic lines used to assess the contribution of ontogenetically distinct hematopoietic waves to the macrophage lineage upon tissue injury.
(B) Diagram showing the amputation plan, tail fin of *Tg(fli1a:creERT2;mpeg1:Switch)* were amputated at 2 dpf and macrophages recruitment to the site of injury was analyzed. Representative images are shown at 24 hpa. Scale bar: 100µm.
(C) Diagram showing the counting region in the larvae. Quantification of DsRed and GFP macrophage number at the site of injury at 24 hpa (n=14) and 48 hpa (n=12). Mean ± SEM of the $DsRed^+$ and GFP^+ macrophage number at each time point is shown. $^{****}p \leq 0.0001$.

(D) Diagram showing the amputation plan, tail fin of *Tg(fli1a:creERT2;mpeg1:Switch)* were amputated at 5 dpf and macrophages recruitment to the site of injury was analyzed. Representative images are shown at 24 hpa. Scale bar: 100µm.
(E) Diagram showing the counting region in the larvae. Quantification of DsRed and GFP macrophage number at the site of injury at 24 hpa (n=10) and 48 hpa (n=6). Mean ± SEM of the $DsRed^+$ and GFP^+ macrophage number at each time point is shown. $^{****}p \leq 0.0001$.
(F) Tail fin of *Tg(fli1a:creERT2;mpeg1:Switch)* were amputated at 5 dpf and macrophages recruitment to the site of injury was analyzed. Representative images are shown at 3 hpA. Scale bar: 100µm.
(G) Quantification of DsRed and GFP macrophage number at the site of injury at 3 hpa (n=13). Mean ± SEM of the $DsRed^+$ and GFP^+ macrophage number at each time point is shown (left). Quantification was normalized by the number of total macrophages in the tail of the respective larvae (the sum of peripheral, CHT and recruited macrophages of distinct origins). $^{**}p \leq 0.01$;$^{****}p \leq 0.0001$.

Figure 4: Selective ablation of definitive macrophages does not impair tail fin regeneration in early larvae.

(A) Diagram showing the macrophage ablation and tail fin amputation plan.
(B) Switched *Tg(fli1a:creERT2;mpeg1:Switch)* larvae were treated with DMSO as a control, or metronidazole (MTZ) to ablate definitive macrophages. Treatments were performed from 4 to 6 dpf. Representative images are shown 48 hours after treatments. Scale bars: 100 µm.
(C) Quantification of DsRed and GFP macrophage number in the tail region 48 hours after DMSO (n=9) or MTZ (n=9) treatments. Mean ± SEM of the $DsRed^+$ and GFP^+ macrophage number is shown. $^{****}p \leq 0.0001$.
(D) Switched *Tg(fli1a:creERT2;mpeg1:Switch)* larvae were treated with DMSO as a control, or metronidazole (MTZ) to ablate definitive macrophages. Treatments were performed from 4 to 6 dpf and tail fins were amputated at 5 dpf. Representative images are shown 24 hours after amputation. Scale bars: 100 µm.
(E) Quantification of DsRed and GFP recruited macrophage number in the tail region 24 hours after amputation. Larvae were treated at 4 dpf with either DMSO (n=11) or MTZ (n=20) for 48 hours. Mean ± SEM of the $DsRed^+$ and GFP^+ macrophage number is shown. $^{****}p \leq 0.0001$.
(F) Switched *Tg(fli1a:creERT2;mpeg1:Switch)* larvae were treated with DMSO as a control, or metronidazole (MTZ) to ablate definitive macrophages. Treatments were performed from 4 to 6 dpf and tail fins were amputated at 5 dpf. Representative images are shown 48 hours after amputation. Scale bars: 100 µm.
(G) Quantification of DsRed and GFP recruited macrophage number in the tail region 48 hours after amputation. Larvae were treated at 4 dpf with either DMSO (n=17) or MTZ (n=9) for 48 hours. Mean ± SEM of the $DsRed^+$ and GFP^+ macrophage number is shown. $^{****}p \leq 0.0001$.
(H) Representative images of regenerating tail fins of larvae at 72 hours after amputation. Larvae were treated with either DMSO or MTZ. Scale bars: 100 µm.
(I) Tail fin area quantification of regenerating tail fins at 24 hpa, 48 hpa and 72 hpa in larvae treated with either DMSO or MTZ (24 hpa: DMSO n=21, MTZ n=20; 48 hpa: DMSO n=17, MTZ n=9; 72 hpa: DMSO n=14, MTZ n=9).

Sup. Figure 1: labeling strategy and the labeling efficiency of using thymocytes as a positive read out with *lck*:switch and *coro1a*:switch transgenic lines.
(A) Scheme of the 4-OHT-inducible transgenic lines used to assess the efficiency of the labelling strategy using the *Tg(fli1a:creERT2;lck:Switch)* double transgenic line.
(B) Fluorescent images of EtOH non-switched controls (right) and 4-OHT-induced (left) *Tg(fli1a:creERT2;lck:Switch)* thymocytes at 5 dpf larvae. Representative images are shown. Scale bars, 100 µm.
(C) Quantification of DsRed and GFP fluorescence intensity percentage in the thymic region was measured at 5 dpf (n=14). Mean ± SEM of the $DsRed^+$ and GFP^+ corrected total cell fluorescence (CTCF) percentage is shown. $^{****}p \leq 0.0001$.
(D) Scheme of the 4-OHT-inducible transgenic lines used to assess the efficiency of the labelling strategy using the *Tg(fli1a:creERT2;coro1a:Switch)* double transgenic line.
(E) Fluorescent images of EtOH non-switched controls (right) and 4-OHT-induced (left) *Tg(fli1a:creERT2;coro1a:Switch)* thymocytes at 3 dpf embryos. Representative images are shown. Scale bars, 100 µm.
(F) Quantification of DsRed and GFP fluorescence intensity percentage in the thymic region was measured at 3 dpf (n=8). Mean ± SEM of the $DsRed^+$ and GFP^+ corrected total cell fluorescence (CTCF) percentage is shown. $^{****}p \leq 0.0001$.

Supp videos related to figure 1. Fluorescence imaging of 4-OHT-induced *Tg(fli1a:creERT2;globin:Switch)* embryos and larvae over a time course of 2- 8 dpf. Videos are assembled from different Z-stacks projections at each defined developmental stage.

Supp Fig.2. Quantification of GFP+ microglia in the head region at 2 dpf embryos. related to Fig.2

(A) Fluorescent images of EtOH non-switched controls (right) and 4-OHT-induced (left) *Tg(fli1a:creERT2;mpeg1:Switch)* head regions in the developing embryos at 2 dpf. Representative images are shown Scale bar: 100µm.

(B) Quantification of GFP+ macrophage number in the head at 2 dpf (n=6). Mean ± SEM of the and GFP^+ macrophage number is shown.

Supp fig 3. Ontogenetically distinct macrophages recruitment after tail injury at different developmental stages. related to fig 3

(A) tail fin of *Tg(fli1a:creERT2;mpeg1:Switch)* were amputated at 2 dpf and macrophages recruitment to the site of injury was analyzed. Representative images are shown at 48 hpA. Scale bar: 100µm.

(B) tail fin of *Tg(fli1a:creERT2;mpeg1:Switch)* were amputated at 5 dpf and macrophages recruitment to the site of injury was analyzed. Representative images are shown at 48 hpA. Scale bar: 100µm.

(C) Switched *Tg(fli1a:creERT2;mpeg1:Switch)* larvae were treated with DMSO as a control, or metronidazole (MTZ) to ablate definitive macrophages. Treatments were performed from 4 to 6 dpf and tail fins were amputated at 5 dpf. Representative images are shown 72 hours after amputation. Scale bars: 100 µm.

(D) Quantification of DsRed and GFP recruited macrophage number in the tail region 72 hours after amputation. Larvae were treated at 4 dpf with either DMSO (n=14) or MTZ (n=9) for 48 hours. Mean ± SEM of the $DsRed^+$ and GFP^+ macrophage number is shown.